The mechanism underlying asymmetric bending of lateral petals in Delphinium (Ranunculaceae)

Hanghang Zhang, Fang Xue, Liping Guo, Jie Cheng, Florian Jabbour, Pierre-Emmanuel Dupasquier, Yanru Xie, Peng Zhang, Yijia Wu, Xiaoshan Duan, et al.

Article

Current Biology

The mechanism underlying asymmetric bending of lateral petals in *Delphinium* (Ranunculaceae)

Graphical abstract

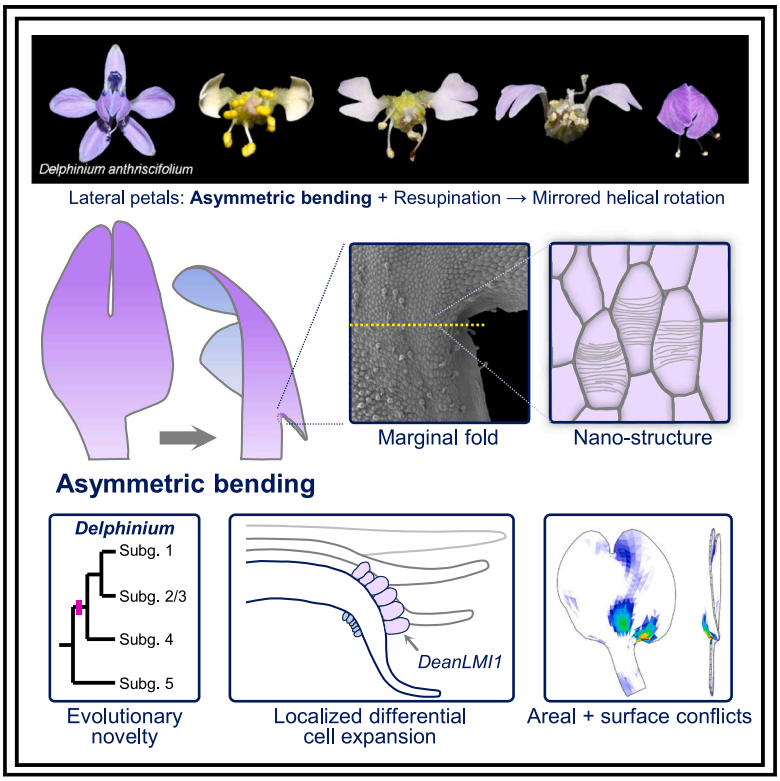

Authors

Hanghang Zhang, Fang Xue, Liping Guo, ..., Xiaoshan Duan, Hongzhi Kong, Rui Zhang

Correspondence

ruizhang@nwafu.edu.cn

In brief

During the flower opening of the *Delphinium*, the pair of lateral petals (if present) display a peculiar movement, the mirrored helical rotation. Zhang et al. discover that an evolutionary novelty, petal asymmetric bending, further reinforces such movement. Using *D. anthriscifolium* as a model, they provide a comprehensive portrait of this trait.

Highlights

- A marginal, wedge-shaped fold responds for petal asymmetric bending
- The fold is due to greater expansion of cell width on localized adaxial epidermis
- The fold is also associated with the specialized array of cell wall nano-structure
- A class I HD-Zip gene, *DeanLMI1*, plays important roles in petal asymmetric bending

Zhang et al., 2024, Current Biology *34*, 755–768
February 26, 2024
https://doi.org/10.1016/j.cub.2024.01.004

CellPress

Current Biology

CellPress
OPEN ACCESS

Article

The mechanism underlying asymmetric bending of lateral petals in *Delphinium* (Ranunculaceae)

Hanghang Zhang,[1,8] Fang Xue,[1,8] Liping Guo,[1,8] Jie Cheng,[2,3,4] Florian Jabbour,[5] Pierre-Emmanuel DuPasquier,[6] Yanru Xie,[1] Peng Zhang,[1] Yijia Wu,[1] Xiaoshan Duan,[1] Hongzhi Kong,[2,3,7] and Rui Zhang[1,9,*]

[1]College of Horticulture, Northwest A&F University, Yangling, Shaanxi 712100, China
[2]State Key Laboratory of Systematic and Evolutionary Botany, Institute of Botany, Chinese Academy of Sciences, Beijing 100093, China
[3]China National Botanical Garden, Beijing 100093, China
[4]Department of Computational and Systems Biology, John Innes Centre, Norwich Research Park, Colney Lane, Norwich NR4 7UH, UK
[5]Institut de Systématique, Evolution, Biodiversité (ISYEB), Muséum National d'Histoire naturelle, CNRS, Sorbonne Université, EPHE, Université des Antilles, Paris 75005, France
[6]Office National des Forêts, 11 C rue René Char, Dijon 21000, France
[7]University of Chinese Academy of Sciences, Beijing 100049, China
[8]These authors contributed equally
[9]Lead contact
*Correspondence: ruizhang@nwafu.edu.cn
https://doi.org/10.1016/j.cub.2024.01.004

SUMMARY

During the process of flower opening, most petals move downward in the direction of the pedicel (i.e., epinastic movement). In most *Delphinium* flowers, however, their two lateral petals display a very peculiar movement, the mirrored helical rotation, which requires the twist of the petal stalk. However, in some lineages, their lateral petals also exhibit asymmetric bending that increases the degree of mirrored helical rotation, facilitating the formation of a 3D final shape. Notably, petal asymmetric bending is a novel trait that has not been noticed yet, so its morphological nature, developmental process, and molecular mechanisms remain largely unknown. Here, by using *D. anthriscifolium* as a model, we determined that petal asymmetric bending was caused by the localized expansion of cell width, accompanied by the specialized array of cell wall nanostructure, on the adaxial epidermis. Digital gene analyses, gene expression, and functional studies revealed that a class I homeodomain-leucine zipper family transcription factor gene, *DeanLATE MERISTEM IDENTITY1* (*DeanLMI1*), contributes to petal asymmetric bending; knockdown of it led to the formation of explanate 2D petals. Specifically, *DeanLMI1* promotes cell expansion in width and influences the arrangement of cell wall nano-structure on the localized adaxial epidermis. These results not only provide a comprehensive portrait of petal asymmetric bending for the first time but also shed some new insights into the mechanisms of flower opening and helical movement in plants.

INTRODUCTION

Unlike most animals that can move without constraint, land plants are rooted in place during most of their life. Despite this, some of their tissues, organs, or single cells can sense and respond to environmental cues through movement to optimize their survival, growth, and reproduction. For example, the leaves of Venus flytrap (*Dionaea muscipula* J. Ellis, Droseraceae) can fold very fast when their sensitive hairs are triggered by insects, and the single cell of pollen tube can grow through the style to deliver sperm to the ovule. These interesting phenomena have intrigued biologists since Darwin who wrote *The Power of Movement in Plants*.[1] In the past century, the plant movements have been extensively investigated, which can be defined as the process of changes in the spatial orientation or conformation of an organ or its parts.[2] Depending on the stimuli signals and corresponding driving forces, plant movements can be classified into three main types.[2,3] The first, termed tropic movement, is induced by directional signals, such as light or gravity. For example, the light-directed movement (i.e., phototropism) of stems is controlled by irreversible differential growth rate on both sides. The second, termed nastic movement, is invoked by non-directional factors, such as temperature or touch. For instance, the touch-stimulated movement (i.e., thigmonasty) of *Mimosa pudica* L. (Fabaceeae) leaves is caused by reversible changes in turgor pressure of the pulvinus. The third, termed autonomous movement, is synchronized by a circadian cycle under the control of biological clock, such as the 24-h diurnal rhythms of light and dark periods (i.e., photoperiodism), such as the opening and closing of some leaves, flowers, and stomata.

Of the various kinds of plant movements, flower opening is undoubtedly one of the most attractive. It can expose the stamens and carpels to facilitate cross-pollination, a crucial prerequisite for reproduction of most species.[4] Notably, this process is largely driven by the movement of floral organs, particularly the petals or tepals (hereafter collectively called petals). Therefore, uncovering the processes, patterns, and mechanisms of petal movement is

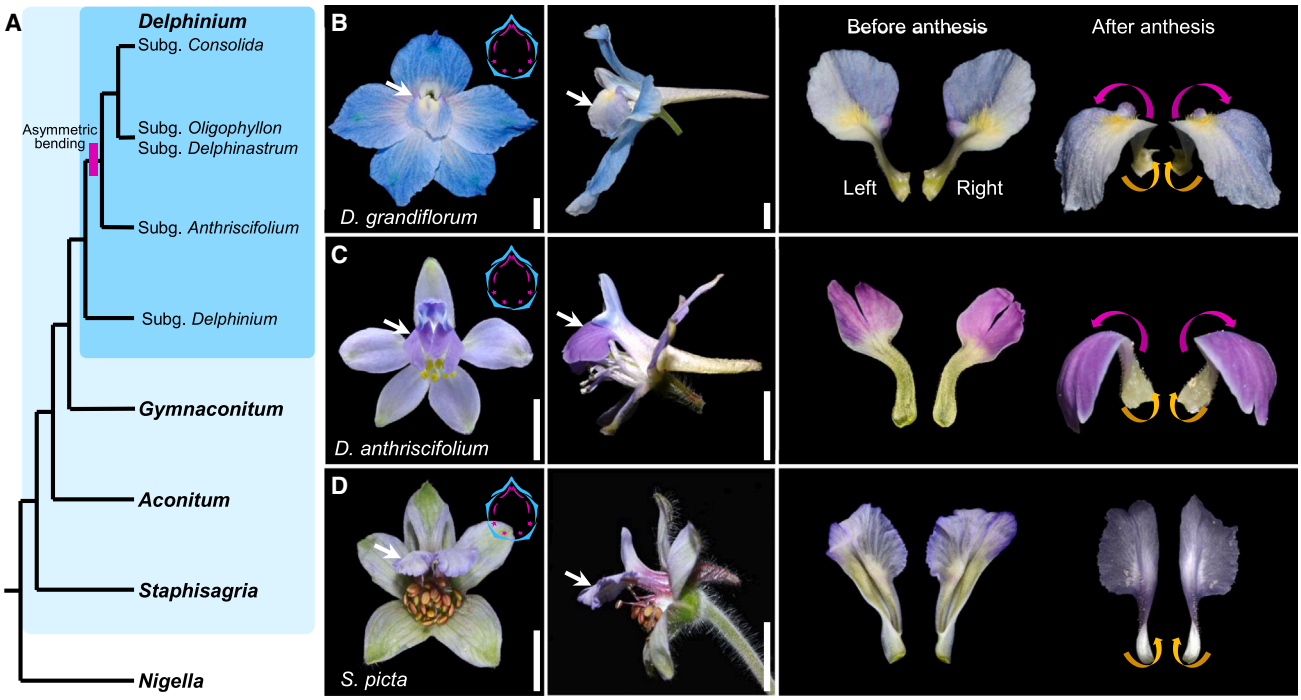

Figure 1. Evolution of asymmetric bending of lateral petals and its effects on the mirrored helical rotation

(A) A simplified phylogenetic tree of the Delphinieae, adopted from previous studies,[17–19] showing the evolution of petal asymmetric bending. The light and deep blue boxes indicate the tribe Delphinieae and the genus *Delphinium*, respectively. The pink block highlights the possible origination node of petal asymmetric bending.

(B–D) Representative species showing their front views (left column), side views (middle column), and the degrees of helical rotation of lateral petals (right column). Perianth diagrams were shown in the top right corner of the first column, with the blue and pink colors representing sepals and petals, respectively. White arrows in the first two columns indicate the lateral petals. The orange and purple crooked arrows denote the orientation of stalk resupination and blade asymmetric bending, respectively. Note that the pair of *Staphisagria picta* petals at the bottom right corner shows the back view to display the changes in its spatial conformation. Scale bars: 5 mm.

See also Figures S1 and S2, Table S1, and Video S1.

critical for a comprehending of flower development and evolution, and for the production guidance of ornamental plants. It has been proposed that petal movement can be achieved through different ways. The most commonly seen petal movement can be attributed to the differential growth between the abaxial and adaxial sides, in response to various external and internal factors, such as temperature, humidity, water, circadian clock, and hormones.[4,5] In addition, the *Lilium* (Liliaceae) petal opening is achieved predominantly through edge growth,[6] whereas the *Ipomoea* (Convolvulaceae) corolla opening (and closing) is due to differences in cell expansion on both sides of the midrib rather than the lamina.[7] Nevertheless, the molecular mechanisms underlying petal movement are not well understood. A recent study showed that the rose (*Rosa hybrida* Vill., Rosaceae) petal movement is driven by the asymmetric growth at the petal base, which is controlled by a *PETAL MOVEMENT-RELATED PROTEIN1-ANAPHASE-PROMOTING COMPLEX 3b* (*RhPMP1-RhAPC3b*) module in an ethylene-dependent manner.[8]

It is worth noting that during flower opening, most petals move downward in the direction of the pedicel (i.e., epinastic movement).[2] However, there are some taxa, such as the genus *Delphinium* (Ranunculaceae), exhibiting a more complex and peculiar petal movement. The mature flowers of *Delphinium* are highly specialized and zygomorphic; they generally have five petaloid sepals (one dorsal spurred, two lateral and two ventral non-spurred) and four synorganized true petals (two dorsal spurred and two lateral non-spurred).[9–12] During the process of flower opening, their petaloid sepals show epinastic movement similar to petals of many other species. Interestingly, their two lateral non-spurred petals display another type of movement, the mirrored helical rotation. That is, for a flower facing the observer, the left petal rotates anticlockwise, while the right one rotates clockwise.[13] As a result, unlike the exposure of reproductive organs mentioned above, the two lateral petals ultimately cover the stamens, carpels, and the entrance of the spurred petals when the flowers are fully opened (Figures 1B and 1C; Video S1).[14] More importantly, it has been proposed that the two lateral petals (hereafter called petals for short, unless otherwise stated) of some *Delphinium* species may have critical contributions to pollination success: (1) functioning as a mark to attract and guide pollinators,[15,16] (2) providing a landing platform with increased rigidity for pollinators,[13] (3) covering the entrance of the spurred petals and the stamens to prevent nectar from drying and increase the duration of insect visits,[13] and (4) acting as a biomechanical filters to screen the effective visitors who are strong enough to press the petals so as to access the reproductive organs.[14] These adaptive functions of the two petals are all associated with the mirrored helical rotation.

Previous studies have shown that the lateral petals of *Delphinium* (except for subg. *Consolida*, whose flowers are devoid of lateral petals) and *Staphisagria* (the earliest-diverging genus of the tribe Delphinieae) are composed of a proximal stalk/claw (hereafter called stalk throughout) and a distal blade, in which the stalk can twist about 180° (i.e., resupination) before anthesis (Figures 1B–1D).[13,20] Nevertheless, the resupination is necessary but not sufficient for the petal helical rotation. Suppose that if the petal stalks were our arms and the petal blades were our palms, when the left and right arms (stalks) rotate to the left and right, respectively, the pair of palms (blades) would fail to cover our chest (stamens, carpels and the entrance of the spurred petals), as observed in *Staphisagria* (Figure 1D). This suggests that the more dramatic helical rotation requires additional conditions. Close inspection of the petals in two species, *D. grandiflorum* L. and *D. anthriscifolium* Hance representing two different subgenera, we unexpectedly found that the junction of the stalk and blade experiences a kind of asymmetric bending through 90° during flower opening (Figures 1B and 1C; Video S1). This explains why the pair of petals can finally cover the reproductive organs and the entrance of spurred petals, hence greatly contributing to the final floral appearance.

More interestingly, when the character states of presence or absence of petal asymmetric bending were mapped onto the phylogenetic tree of the Delphinieae, we found that this trait possibly originated at least once. The origin node with high possibility was after the divergence of subg. *Delphinium* from its sister clades, although another node within the subg. *Delphinium* could not be excluded (Figures 1A and S2; Table S1). This result suggested that petal asymmetric bending was a morphological innovation. However, this trait has not been noticed yet, so that its morphological nature, developmental process, and molecular mechanisms remain unknown. In this study, using *D. anthriscifolium* as a model, we addressed these questions through extensive morphological, anatomical, developmental, computational, comparative transcriptomic, as well as gene expression and functional studies. These results not only provide a comprehensive portrait of petal asymmetric bending but also shed some new insights into the mechanisms of flower opening and helical movement in plants.

RESULTS

Morphological and anatomical nature of petal asymmetric bending

To understand the morphological basis of petal asymmetric bending, we performed morphological and anatomical studies for *D. anthriscifolium* petals. We found that the distal petal blade shows internal asymmetry and is bifurcated into two lobes. The dorsal lobe has a thinner lamina, smoothly connecting with the stalk, while the ventral lobe has a protruded lamina at its base, forming an obvious hinge with the adjacent stalk (Figures 2A and 2C). Interestingly, further investigation through scanning electron microscopy (SEM) revealed that there is a wedge-shaped fold at the hinge (Figures 2B and 2D). However, in *Staphisagria picta* petals that do not perform asymmetric bending, we observed an explanate margin rather than a fold at the hinge (Figures S3E–S3L). It is not difficult to imagine that at the margin of a printing paper, if a small fraction had a wedge-shaped fold, the whole paper would definitely deform and bend out of the originally 2D plate due to mechanical stress. Therefore, we speculated that this marginal fold may be the reason for petal asymmetric bending.

To further understand how such a marginal fold was formed, we first observed and compared the epidermal cells between this and other regions. We found that the cells on two sides of the blade are distinct (Figures S3A and S3B). The adaxial side is distinguished by conical cells with different shapes, while the abaxial side has pavement cells in the central region and elongated cells in the basal region (Figures S3A and S3B). More importantly, we found that in the region close to the hinge, the adaxial epidermal cells are significantly wider than the abaxial ones in width (Figures 2B2 vs. 2D2′), with the median values of cell width being 22.24 and 11.90 μm ($p = 1.61E-18$, Figure 2E), respectively. This, together with the differences in cell lengths, made the cell anisotropy of adaxial epidermis lower than the abaxial ones (Figure 2E). Meanwhile, on the adaxial side of the intermediary region connecting the blade and stalk, the cells close to the hinge are significantly wider than the other end, with the median values of cell width being 22.24 and 18.65 μm ($p = 2.19E-04$, Figure 2F). In the region far from the hinge, however, the epidermal cells between the two sides show no significant difference in width (Figure S3D). Moreover, we also found that the surfaces of adaxial epidermal cells have stripe-shaped nanoridges, but those close to and far from the hinge display different orientations, with the former's perpendicular to while lateral's horizontal to the longitude cell axis (Figures 2B1 and 2B2). These results suggest that in the region close to the hinge of the adaxial side, greater expansion in cell width accompanied by the specialized array of nano-structure may be important for petal asymmetric bending.

To further confirm the above hypothesis, we conducted anatomical observation by transverse semi-thin sectioning of petals along the intermediary region (Figure 2G). We found that (1) this region is composed of tightly packed epidermis, as well as inner parenchyma cells and three embedded vascular bundles; (2) the cell numbers between the adaxial and abaxial epidermis show no obvious difference (Figures 2G and 2H), suggestive of their negligible roles in the petal bending. We also compared the cell widths between the adaxial and abaxial epidermis along the sections. The result showed that from the dorsal end to the middle part, the cell widths of both sides gradually and synchronously increase with no obvious difference, while from the middle to the ventral part approaching the hinge, the differences between the two sides become more and more pronounced (Figure 2I). Specifically, the cell width of the abaxial side decreases dramatically compared with that of the adaxial side (Figure 2I), yielding the biggest difference in the region close to the hinge. Taken together, these results suggest that in the region close to the hinge, it is the differences in cell width between the adaxial and abaxial epidermis that made the marginal fold, which further promoted petal asymmetric bending.

Developmental basis of petal asymmetric bending

To understand how petal asymmetric bending of *D. anthriscifolium* was generated through development, we performed time course morphological and anatomical studies. At stage 10 (S10) and

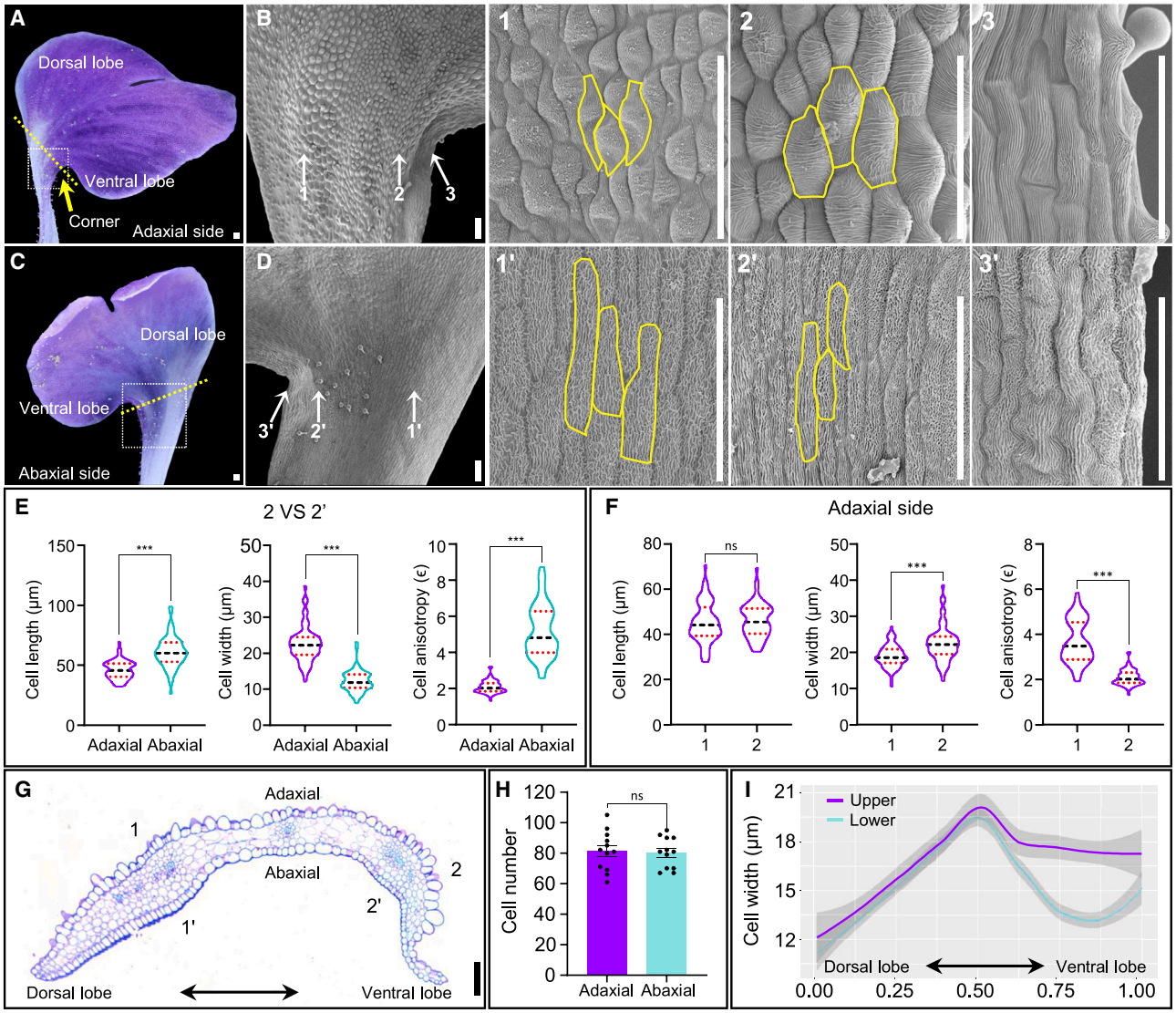

Figure 2. Morphological and cellular bases of petal asymmetric bending of *D. anthriscifolium*

(A–D) The mature left petal showing the adaxial side (A and B) and abaxial side (C and D) of the blade. Note that the images in (A) and (C) were captured from the same petal. The yellow arrow indicates the hinge. The white dashed squares in (A) and (C) highlight the asymmetric bending regions that are further zoomed-in by SEM (B and D), and the yellow dashed lines indicate the intermediary region used for transverse semi-thin sectioning shown in (G). Images 1–3 and 1′–3′ present different epidermal cell types corresponding to the numbered regions in (B) and (D), respectively, with the cell outlines being marked with yellow circled lines.

(E and F) Epidermal cell measurements and comparisons between different regions (n = 60). Median and quartile values are indicated by black and red dashed lines, respectively. Significant levels (p values) were evaluated using t test.

(G) Transverse semi-thin section corresponding to the highlighted yellow lines in (A) and (C).

(H and I) Cell number (H) and cell width (I) comparisons between adaxial and abaxial epidermis along transverse semi-thin sections (n = 12), with the cell numbers in (I) normalized to 1.0. Significant levels (p values) were evaluated using t test. Data in (H) are mean ± SE. Scale bars: 100 μm.

See also Figure S3.

S11 of floral development,[13,21] the hinge region showed neither deformation in shape nor epidermal cell differentiation on both sides (Figures 3A and 3B). At S12, the hinge began to fold, with evident cell expansion being observed (Figure 3C). From S13 on, the folded hinge has become more and more obvious (Figures 3D–3F). Accordingly, the epidermal cells on both sides were extensively expanding. However, the adaxial ones showed greater expansion in width while the abaxial ones in length, and they finally differentiated into the spindle-shaped conical cells and elongated cells, respectively (Figures 3D–3F). In addition, on the adaxial epidermal cells close to the hinge, stripe-shaped nanoridges perpendicular to the longitudinal axis were also gradually forming (Figures 3D–3F).

To quantify the dynamics of cell expansion during petal development, we measured the cell lengths and widths of both sides close to the hinge. Indeed, the increase in cell widths was faster on the adaxial side than the abaxial side, whereas the increase of cell lengths was opposite (Figures 3G and 3H). In particular,

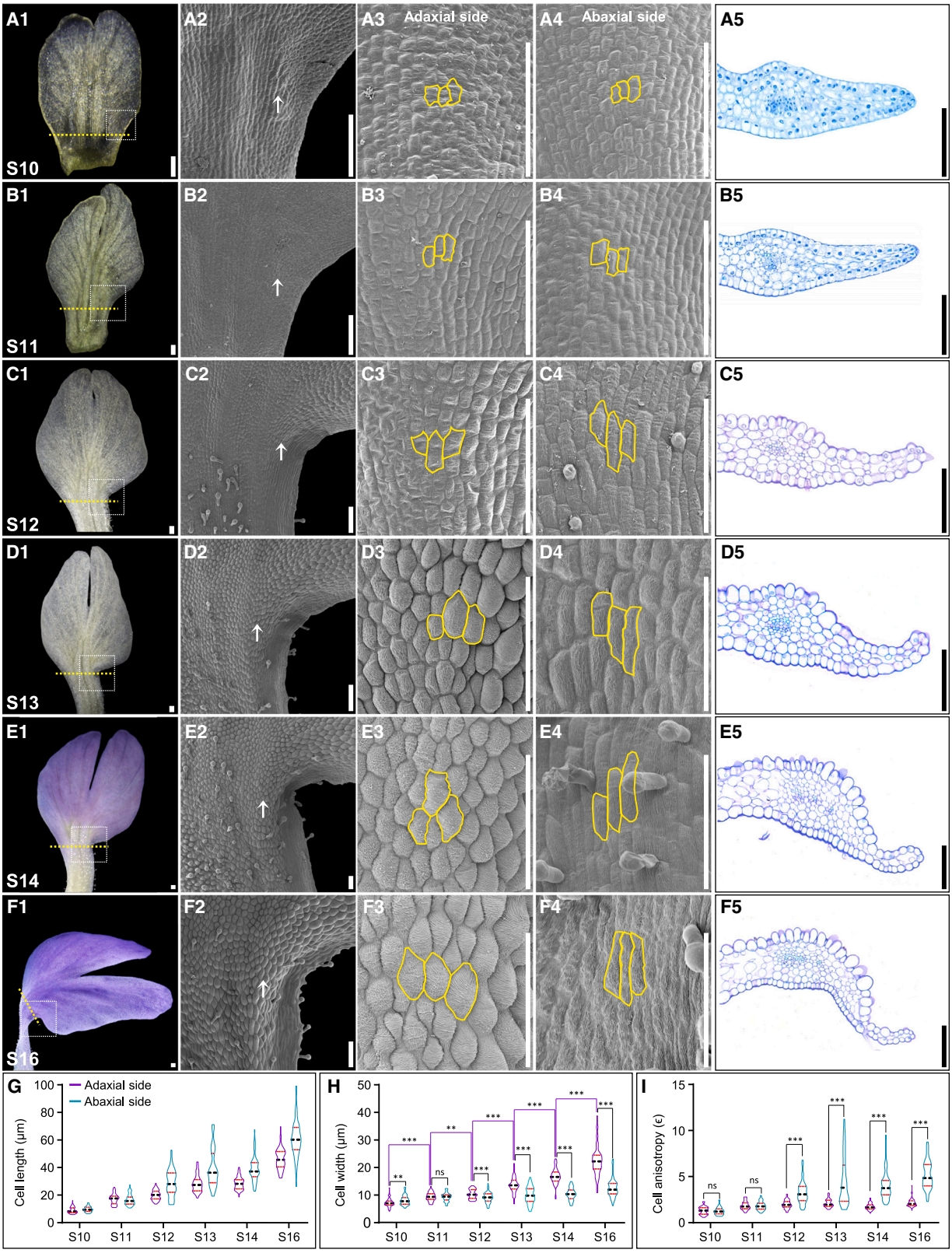

(legend on next page)

starting from S12, cells from the adaxial epidermis became significantly wider than those of the abaxial side at each stage-pair (Figure 3H), which is consistent with the results of transverse semi-thin sectioning for the intermediary region (Figure S4). Finally, these dynamic changes in cell size resulted in significant differences in cell anisotropy (Figure 3I). Meanwhile, the transverse semi-thin sectioning also revealed that from S10, the cell numbers between the adaxial and abaxial epidermis did not exhibit obvious differences (Figure S4). All together, these results demonstrated that an extensive increase in cell width of the adaxial epidermis close to the hinge during development was likely associated with the formation of the marginal fold and the resultant petal asymmetric bending.

To understand how the differential growth controls petal asymmetric bending, we modeled the petal growth under a polarity-based system (Figures 4A and 4B).[22] Previous studies have shown that out-of-plane deformation can be generated through tissue conflicts driven by specified growth.[23] By surveying the cellular morphological dynamics during petal development, we hypothesized that areal and surface conflicts may be the key. To test this hypothesis, we first modeled the petal growth with the default parameters,[24] which gave rise a planar petal with a stalk at the base and a bifurcated blade at the top at the final state (Figures 4C–4E; Video S2, left). Then, based on the default model, we tested the areal conflict by introducing a growth promoting factor to the region close to the hinge on both the adaxial and abaxial sides (Figure 4F). This modeling process also generated a planar petal, with no bend or fold being observed because of the same specified growth rate on both sides (Figures 4G and 4H; Video S2, middle). Next, we further introduced surface conflict by setting the growth promoting factor just to the adaxial side of the same region (Figure 4I). This time, the model predicted an out-of-plane structure, in which the hinge folded due to the higher specified growth rate and residual bend rate at the adaxial side (Figures 4J and 4K; Video S2, right). Thus, the combination of morphological quantifications and computational modeling suggests that the petal asymmetric folding requires the areal and surface conflicts, thereby producing regionally differential growth close to the hinge.

Identification of the genes associated with petal asymmetric bending

To understand the molecular mechanisms underlying petal asymmetric bending, we conducted digital gene expression (DGE) analyses for *D. anthriscifolium*. The dorsal spurred and lateral non-spurred petals at four developmental stages (S9, S10, S12, and S16) were sampled for RNA sequencing (Figure 5A; Data S1A), respectively. For comparison, the three sub-types of sepals (i.e., dorsal spurred, lateral, and ventrally non-spurred), stamens and carpels at corresponding stages, as well as leaves and bracts that are just underneath the S9 floral buds were also included (Figure 5A). The results of correlation and principal-component analyses showed that (Figures S5A and S5B): (1) for each sub-type of sepals or petals, the relationships were high just between S9 and S10, but rather low between other stage pairs; (2) the relationships among the sub-types of sepals or petals were also very high at S9 and S10 but much lower at later stages, in accordance with the process of their morphological differentiation along the dorsoventral axis of flowers.

To understand the uniqueness of the petals (including both the spurred and non-spurred), we identified 295 and 1,041 genes that were specifically and preferentially expressed in petals, respectively (Figures 5B and S5C; Data S1B and S1C). For these genes, we furthermore compared their expressions between the dorsal and lateral petals and finally identified 287 and 84 significantly up-regulated genes in the former and latter ones, respectively (Figures 5C and S5D–S5G; Data S2A), with each including many well-known regulators involved in petal development. The former ones contained the petal identity gene *DeanAPETALA3-3* (*DeanAP3-3*),[21] a homolog related to floral dorsal identity determination named *DeanRADIALIS2-1* (*DeanRAD2-1*),[25] and genes whose homologs are involved in lateral organ morphogenesis, such as *DeanPRESSED FLOWER* (*DeanPRS*).[26] The latter ones, however, included the *DeanCYCLOIDEA1a* (*DeanCYC1a*) and *DeanDIVARICATA2-3* (*DeanDIV2-3*) genes specifying the floral ventral and lateral identities,[21] and a *LATE MERISTEM IDENTITY1* homolog (*DeanLMI1*) sculpturing lateral organ shapes.[27–31] The genes showing significantly higher expression levels in lateral petals possibly contain the ones associated with petal asymmetric bending.

Effects of *DeanLMI1* on petal asymmetric bending

Of these candidates, *DeanLMI1*, a class I HD-Zip family transcription factor gene, captured our special attention due to its preferential expression in petals, especially in lateral petals (Figure 5D). Another reason is that its counterparts in many other species play key roles in lateral organ morphogenesis (Figure S6A).[27–31] To gain some insights into its precise spatiotemporal expression, we first performed a quantitative reverse-transcription PCR (RT-qPCR) experiment on dissected lateral petals and found that this gene showed higher expression levels in the stalk and hinge relative to the blade (Figures 5E and 5F). We further conducted *in situ* hybridization for this gene. At S4 of floral development, its expression was specifically detected in all the petal primordia (Figures 6A and 6B). This expression pattern was sustained to S6, when the eight petal primordia had not differentiated yet (Figures 6C and 6D). At S8 and S9, however, with the differentiation of petal primordia along the dorsoventral axis, its

Figure 3. Petal asymmetric bending through development

(A–F) Petals at different stages (S10–S16) displayed with stereomicroscope (the left column), SEM (the middle three columns), and transverse semi-thin sections (the right column). The bending regions are highlighted with white dashed rectangles and zoomed-in by SEM (A2–F2), in which the white arrows point to the regions showing cell types and sizes on the adaxial (A3–F3) and abaxial (A4–F4) epidermis, with the cell outlines being marked with yellow circled lines. The yellow dashed lines in the left column indicate the corresponding transverse semi-thin sections shown in the right column.

(G-I) Comparisons of epidermal cell length (G), width (H), and anisotropy (I) for the regions between A3–F3 and A4–F4 (n = 60). Median and quartile values are indicated by black and red dashed lines, respectively. Significant levels (p values) were evaluated using t test. Scale bars: 100 μm.

See also Figure S4.

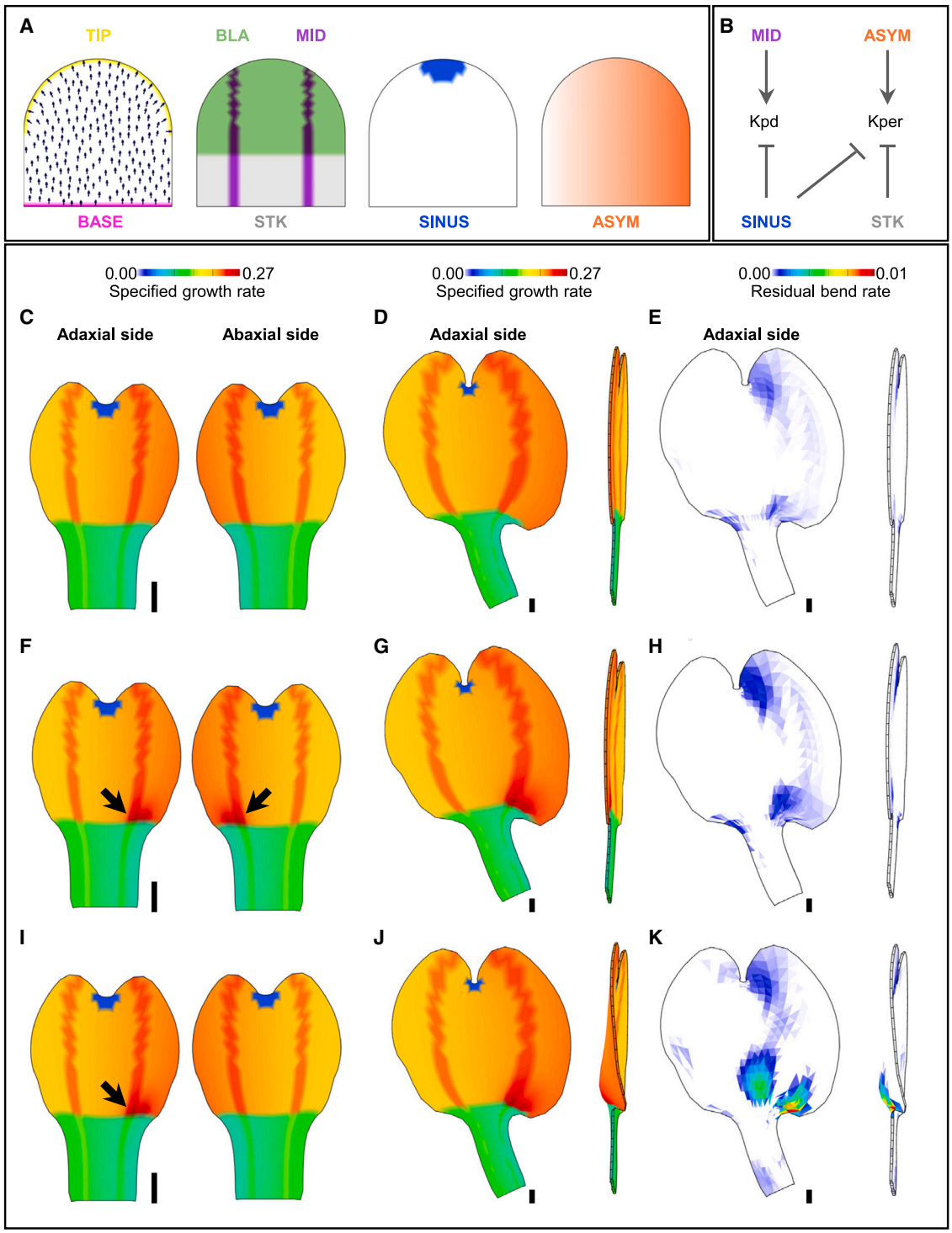

Figure 4. Computational modeling of petal asymmetric bending

(A) Initial setup of the model. This model sets a proximodistal polarity that runs from the base (magenta) to the distal tip (yellow) and five spatially distributed factors: BLA (green), MID (purple), STK (gray), SINUS (blue), and ASYM (orange).

(B) Growth regulatory network of the petal growth model. *K*pd (parallel to the proximodistal polarity field) and *K*per (perpendicular to the former one) determine the elongating and widening of a planar structure, respectively. STK, MID, SINUS, and ASYM were used to regulate the two growth rates of *K*pd and *K*per.

(legend continued on next page)

expression was maintained at high levels in the dorsal and lateral petals but obviously decreased in the ventral reduced petals (Figures 6E–6J). At S10/11, just before the hinge folds, its expression decreased in both the dorsal and lateral petals (Figures 6K–6M). Notably, we found that the spatial distribution of *DeanLMI1* signals in lateral petals were heterogenetic. On the dorsal part, it was mainly distributed to the intermediary region where surrounds the hinge; on the ventral part, however, it was restricted to the basal stalk (Figures 6N and 6O). Moreover, when observed from the side view of the hinge region, this gene showed a gradient expression from the adaxial to the abaxial side (Figures 6N3 and 6N4).

To further uncover the function of *DeanLMI1*, we attempted to knock down its expression by using the virus-induced gene silencing (VIGS) technique with the *Tobacco rattle virus* (TRV) construct, i.e., TRV2-*DeanANS*-*DeanLMI1*, in which the *DeanANTHOCYANIDIN SYNTHASE* (*DeanANS*) was used as the marker of gene silencing (Figures S6B–6D). Compared with the TRV2-*DeanANS*-treated plants (i.e., mock), the TRV2-*DeanANS*-*DeanLMI1*-treated plants with strong phenotypic changes (here after termed *ans-lmi1*) exhibited lateral petals that were no longer bent such that they could not cover the stamens and carpels (Figures 7A and 7B), while the petal stalk resupination and other floral organs remained largely unaffected (Figures S6E and 6F). In particular, we also found that in some flowers, one lateral petal that was strongly silenced could not bend whereas the other unaffected one could (Figure 7C; Table S2). In accordance with this, very low expression levels of *DeanLMI1* were detected in lateral petals with strong phenotypic changes (Figure S6K), indicating that the silenced phenotypes were indeed the result of downregulation of *DeanLMI1*.

Further inspection of the micro-structures revealed some morphological and anatomical defects in *ans-lmi1* petals. First, under the SEM, we found that the hinge was folded with an acute angle in mock petals, similar to that of the wild type (WT) but was explanate with an obtuse angle in *ans-lmi1* petals (Figures 7D and 7G). Second, on the adaxial epidermis close to the hinge, the cell width of *ans-lmi1* petals was significantly narrower than those in the mock (Figures 7E, 7H, and 7J). On the abaxial epidermis, however, the cell width showed no obvious difference between the mock and *ans-lmi1* petals (Figures 7F, 7I, and 7J). Moreover, the results of semi-thin sectioning not only confirmed the above observations but also showed that the cell numbers along transverse sections were not significantly different (Figures 7L–7O). Third, it is worth to note that on the adaxial epidermis close to the hinge, the cell surface of mock petals had stripe-shaped nanoridges perpendicular to the longitudinal cell axis, while that of *ans-lmi1* petals had irregular nanoridges, suggestive defects in the nano-structures (Figures 7E and 7H). Taken together, these results provide strong evidence that the *DeanLMI1* gene contributes to petal asymmetric bending by promoting the cell expansion in width and impacting the matrix of cell nano-structures of a localized group of cells on the adaxial epidermis.

DeanLMI1-mediated programs involved in petal asymmetric bending

To further understand how the *DeanLMI1* gene regulates petal asymmetric bending, we conducted DGE profiling for the mock and *ans-lmi1* petals. Differential gene expression analysis identified 289 and 2,612 up- and down-regulated genes in *ans-lmi1* petals relative to the mock (Data S2B), hinting that *DeanLMI1* mainly had activated roles for the downstream genes. Further examination revealed that the up-regulated genes included the *DeanAP3-1* gene specifying the petal and stamen identities, as well as *DeanGNC1* whose ortholog promotes cell growth (Figure S7A).[32] Of the down-regulated genes, several genes associated with the cell growth, polarity establishment, auxin response, and epidermal cell differentiation were identified (Figure S7A). It is possible that these pathway genes may be regulated directly or indirectly by *DeanLMI1* to influence cell growth.

Of these putative downstream programs, the ones involved in auxin pathway draw our attention because auxin plays important roles in cell proliferation and expansion. We, therefore, hypothesize that the regional distribution of auxin may have important roles in petal asymmetric bending. To test this, we performed exogenous indole-3-acetic acid (IAA) application to the whole abaxial surface of WT lateral petals at S11 and S12 of floral development (Figures S7B–S7I). The results showed that at maturity, petals treated with lanolin (mock) could normally bend (Figures S7B–S7E), while the ones treated with 100-mM IAA no longer bent, thereby exposing the reproductive organs (Figures S7F–S7I). SEM analyses revealed that in the IAA-treated petals, the hinge could still fold but the degree was much weaker than that in mock (Figures S7K and S7N), and the adaxial epidermal cells were not that plump as in the mock (Figures S7L and S7O). In line with this, the cell width of adaxial epidermis close to the hinge was significantly reduced compared with that in the mock (Figure S7P), suggesting that the higher IAA level possibly has negative roles in cell expansion. We also found that in the IAA-treated petals, the stalk could not twist normally as the control (Figures S7J and S7M).

DISCUSSION

Morphology, development, and evolution of petal asymmetric bending

In this study, by using *D. anthriscifolium* as a model, we demonstrated that petal asymmetric bending was due to the formation of a marginal fold at the hinge. This fold was caused by the greater expansion in cell width accompanied with the specialized array of cell wall nanoridges on localized adaxial epidermis. This observation is in line with the notion that the bending of many plant organs depends on local differences in cell expansion followed by tissue deformation, such as the typical apical

(C–K) Modeling results of petal growth from the default model (C–E), the default model incorporated with areal conflict (F–H), and the default model incorporated with areal and surface conflicts (I–K). The areal and surface conflicts were introduced with a growth promoting factor (indicated by bold black arrows) to the region close to the hinge. Heatmaps of specified growth rate were plotted on the time 14.5 (C, F, and I) when ASYM is activated and on the final state of time 24 (D, G, and J). Heatmaps of residual bend rate were plotted on the time 24 (E, H, and K). Scale bars represent the same length in all panels and are in arbitrary units. See also Video S2.

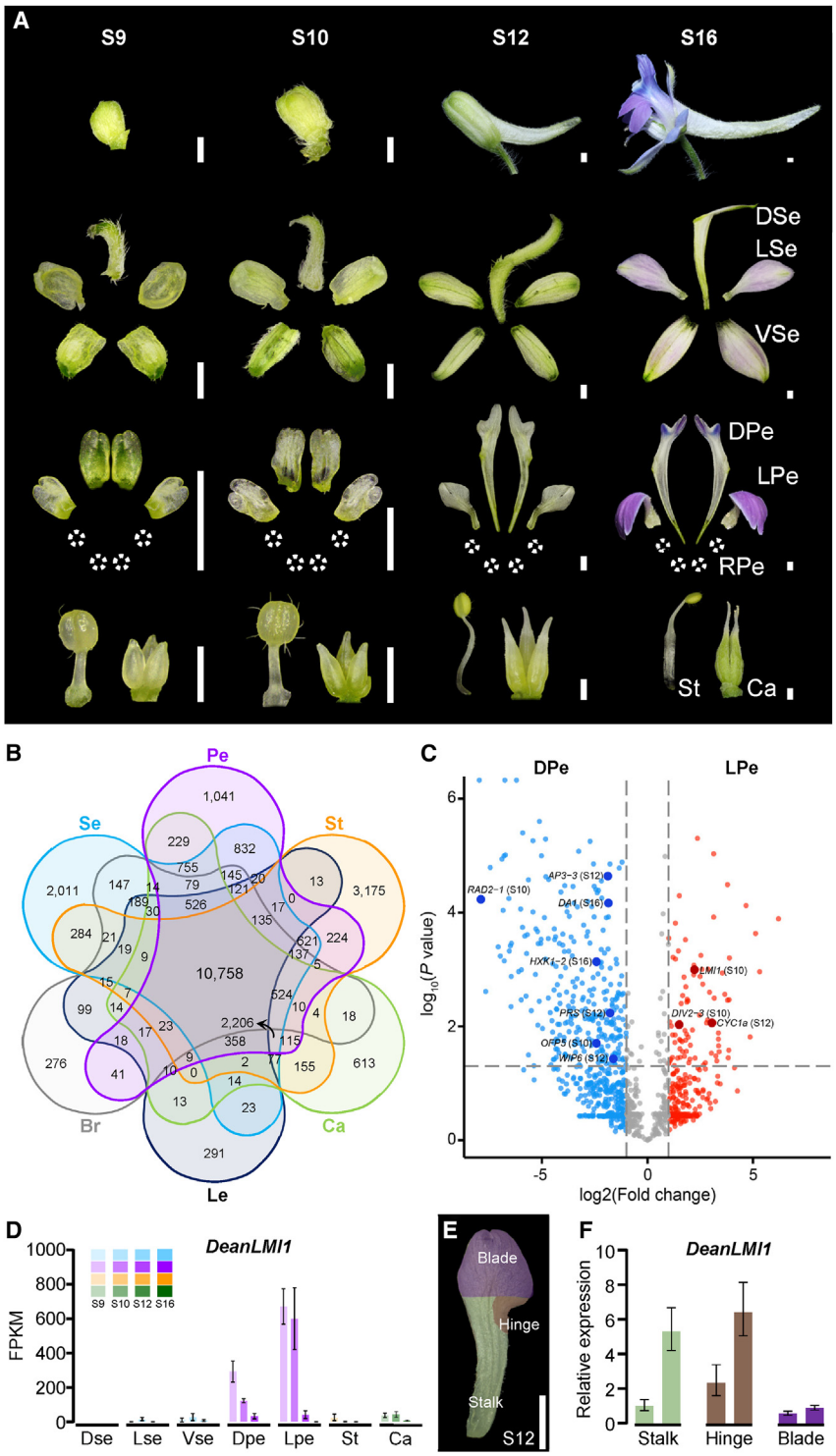

Figure 5. DGE profiling and a candidate associated with petal asymmetric bending

(A) DGE sampling landscape for petals and other organs at representative stages in *D. anthriscifolium*. DSe, spurred dorsal sepal; LSe, lateral sepal, VSe, ventral sepal; DPe, spurred dorsal petal; LPe, lateral petal; RPe, reduced petal represented by white dashed circles; St, stamen; Ca, carpel.

(B) Venn diagram showing the numbers of genes preferentially expressed in different organs.

(C) Of the genes preferentially and specifically expressed in petals, the ones that are differentially expressed between DPe and LPe at each stage are integrated in a volcano plot. For each gene, the values on x and y axes were determined by the highest value at the four stages. The up-regulated genes in dorsal and lateral petals are shown with light blue and light red dots, respectively, while the ones with no significant expression changes are represented by gray dots. Representative genes homologous to the well-known regulators are highlighted with dark and enlarged dots, with the corresponding stage being indicated in the parentheses.

(D–F) Spatiotemporal expression patterns of *DeanLMI1* gene as revealed by DGE profiling (D) and RT-qPCR (E and F). For RT-qPCR, lateral petals were dissected into three parts, stalk, hinge, and blade, each with two biological replicates. Error bars represent standard error (SE) from three technical replicates. Data in (D) and (F) are mean ± SE. Scale bars: 1 mm.

See also Figure S5 and Data S1 and S2.

hook development in *Arabidopsis thaliana* seedlings, with cells on the outer side increasing in size more than those on the inner side.[33]

Moreover, we found that petal asymmetric bending possibly originated at least once within *Delphinium* (Figures 1A and S2). In particular, we noticed that the speciose subgenera of *Delphinastrum/Oligophyllon* retaining this trait contain about 270 species that are mainly distributed in Asia, especially the Himalayas and Southwest China.[34] It has been proposed that the bursts in diversification rate of the two subgenera appear to be associated with the transitions from short-lived to long-lived life cycles in this area.[17] Despite this, it is broadly accepted that changes in the shape and structure of floral organs have profound significance for rapid diversification of corresponding groups.[35,36] In the two subgenera, the evolutionary novelty of asymmetric bending can reinforce the degree of mirrored helical rotation of the paired lateral petals, which contributes to the formation of highly specialized and complex floral appearance,[21] suggestive of its potentially crucial roles in the rapid diversification of the two subgenera.

Molecular mechanisms underlying petal asymmetric bending

In addition to *Delphinium*, the bending or folding of petals can be observed in many other groups, such as Acanthaceae, Bignoniaceae, Boraginaceae, Convolvulaceae, Gentianaceae, Plantaginaceae, and Solanaceae. In the flower of *Antirrhinum*

Figure 6. Spatiotemporal expression of *DeanLMI1*

Results of *DeanLMI1 in situ* hybridization in floral buds at S4 (A and B), S6 (C and D), S8 (E–G), S9 (H–J), and S10/11 (K–M), as well as in lateral petals at S10/11 (N–O). Serial sections of the same floral bud or petal are labeled as serial numbers, with their relative positions being indicated with dashed lines in the perianth diagrams at the top right corner. Expression models of *DeanLMI1* gene are showed in the right diagrams, with the purple color illustrating the expression domain and shades roughly standing for the gene expression levels (the darker, the higher). The gray background in the perianth diagrams indicates the dorsoventral axis, with the darker and lighter regions representing the dorsal and ventral parts, respectively. Black arrowhead indicates the hinge region. Ad, adaxial side; D/V, dorsal/ventral direction of the flower; DPe, spurred dorsal petal; LPe, lateral petal; RPe, reduced petal. Scale bars: 100 μm.

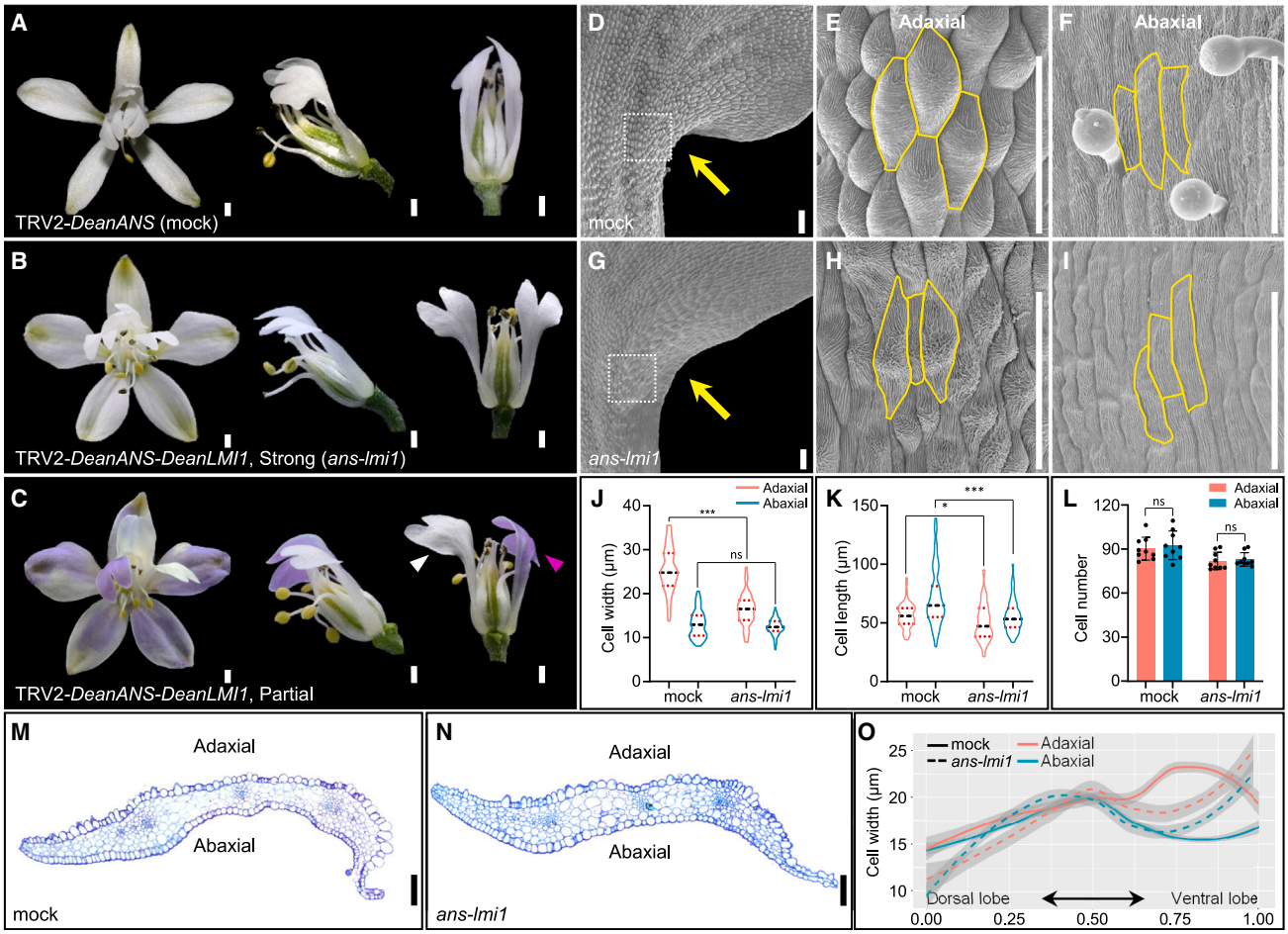

Figure 7. Function of *DeanLMI1* as revealed by virus-induced gene silencing

(A–C) Flowers in the mock (A), TRV2-*DeanLMI1*-treated plants with strong (B) and partial (C) phenotypic changes. In each panel, the whole flowers showing front view and the flowers showing side and top views, with the sepals and spurred dorsal petals that were removed are successively presented from left to right. The white and magenta arrowheads in (C) indicate the strongly silenced and non-silenced petals.

(D–I) Petals under SEM showing the mock (D–F) and strongly silenced (G–I) petals. In (D) and (G), the yellow arrows highlight the phenotypes of the hinge; the white dashed squares correspond to the regions that were magnified in (E and F) and (H and I), with the cell outlines on the adaxial (E and H) and abaxial (F and I) epidermis being marked with yellow circled lines.

(J and K) Comparisons of epidermal cell width (J) and length (K) between the mock and strongly silenced petals (n = 60). Median and quartile values are indicated by black and red dashed lines, respectively. Significance levels (p values) were evaluated using t test.

(L–O) Cellular comparisons between the mock and strongly silenced petals showing the changes in cell numbers (L; n = 9), anatomical structure (M and N), and cell width variations along the transverse sections at the intermediary region in mock and strongly silenced (O) petals (n = 9 in each treatment), with the cell numbers being normalized to 1.0. Data in (L) are mean ± SE. Scale bars: (A–C) 1 mm; (D–I, M, and N) 100 μm.

See also Figures S6 and S7, Data S2B, and Table S2.

(Plantaginaceae), for example, the lower corolla forms a wedge-shaped fold between the palate and lip, thus forming a 3D structure. Previous studies have illustrated that this trait was caused by the *CINCINNATA* (*CIN*) and *CUPULIFORMIS* (*CUP*) genes; they are differentially expressed along the adaxial/abaxial and proximal/distal axes of the lower corolla at later floral developmental stages, creating patches of cell proliferation that contribute to the formation of the fold.[37,38] In *D. anthriscifolium*, however, our results showed that the *DeanLMI1*-mediated petal asymmetric folding is achieved through increasing cell width and influencing the cell wall nano-structures on the adaxial epidermis at the intermediary region closing the hinge. These results, together with the fact that the petal folds have evolved multiple times,[39] suggest that the underlying molecular mechanisms for petal folding may be taxon dependent.

For the roles of *LMI1* orthologs, previous studies have suggested that they have broadly conserved roles in the morphogenesis of lateral organs, such as the compound leaf development in *Cardamine hirsuta* and *Gossypium hirsutum*, the tendril formation in *Pisum sativum*, and the elaborate petal development in *Nigella damascena*.[27,29,30] Nevertheless, unlike the roles of repressing cell division for *LMI1* orthologs,[40] the *DeanLMI1* gene has a role in promoting cell width expansion in lateral petals. In cucumber (*Cucumis sativus*) and *N. damascena*, the *LMI1* orthologs also control trichome development through regulating cell elongation,[30,31] suggestive of a role in increasing cell size. These results

indicate that the functions of *LMI1* orthologs are taxon and context dependent, which rely on specific spatiotemporal expression and interaction patterns. In *D. anthriscifolium*, for instance, the *DeanLMI1* gene has a broader expression domain relative to its very specific phenotypic changes by VIGS (Figures 6 and 7A–7C). This discrepancy suggests that the *DeanLMI1* range of function could be narrowed by other co-factors, which is yet to be investigated.

Biochemical and biomechanical underpinnings of petal asymmetric bending

Previous studies have demonstrated that the asymmetric auxin distribution can influence the mechanical properties and the resultant differential growth.[33] During the apical hook development of *Arabidopsis* seedlings, for example, the high auxin levels on the inner side of the hook result in stiffer cell walls and slower growth, whereas low auxin levels on the outer side have the opposite effect.[41] In particular, this asymmetric auxin distribution is mediated by the polar auxin transport, with the PIN proteins being the key transporters.[41,42] In line with this, our comparative transcriptome analysis revealed that the expression levels of several auxin signaling associated genes[43–47] were significantly down-regulated in the *DeanLMI1*-silenced petals (Figure S7A). This implies that these genes may also promote petal asymmetric bending through asymmetric auxin distribution, which is deserved to study in the future. Moreover, auxin is not the only hormone affecting plant bending; other hormones, such as ethylene, brassinosteroid, and gibberellin and their associated pathway genes have also been found to participate in this process.[48] In rose, for example, the petal opening is driven by ethylene-mediated asymmetric growth of the petal base.[8]

In addition, it is worth noting that on the *D. anthriscifolium* petals, the cell surface of adaxial epidermis close to the hinge has specialized nanoridge matrix perpendicular to the longitudinal cell axis. The nanoridges on the cell surface are exclusively made of cutin, while different cutin matrices have different mechanical strength,[49] and the cuticle overall confers both the elastic and viscous properties for tissues.[50] A previous study in *Ruellia* flowers has confirmed that the petal folds in the corolla throat with their surface nano-structures can significantly provide mechanical support, similar to the folds in corrugated sheets or ribs on ribbed metal rods.[39] In *D. anthriscifolium*, therefore, the specialized nano-structures possibly have similar roles in the fold formation and the following asymmetric bending of petals.

Prospect for the helical movement in plants

Of the many cases of plant movement, helical movement is a very special but widespread type, such as the tendrils of climbing plants, the coiling of pods, and the resupination of leaves and flowers.[51] It has been suggested that the helical movements are driven by helical growth, with the underlying mechanisms being diverse from case to case.[51] First, the cytoskeleton arrangement. In *Arabidopsis*, for example, some mutants with the organs showing helical growth were due to the helically arranged arrays of cortical microtubules, which, in turn, create helical mechanical anisotropy for corresponding cells and tissues.[52,53] Second, the cell wall composition. Again, in *Arabidopsis*, the *rhamnose biosynthesis 1* (*rhm1*) mutants show left-handed helical growth of petal epidermal cells, leading to left-handed twisted petals, which is the result of decrease in the rhamnogalacturonan-I levels.[54] Third, the internal cell composition. In cucumber coiled tendrils, there are two layers of specialized cells similar to the gelatinous fiber (g-fiber), in which the inner layer of the helix shows increased lignification relative to the outer layer, leading to asymmetric contraction of the fiber ribbon.[55] Similarly, in *C. hirsuta*, the very fast curl back of the two valves during explosive pod shatter is due to asymmetric deposition of lignin in endocarp *b* cells, which drives the contraction of epidermal cells so as to release the explosive energy.[56] In this and previous studies, we found that during the flower opening of many *Delphinium* species, the mirrored helical rotations of the paired lateral petals concern two key morphological processes, the twisting of the petal stalk and the asymmetric bending of the petal blade.[13] The latter one has been comprehensively investigated in this study. However, the former one is far from well understood, and uncovering the mechanisms underlying this process will provide some new insights into the helical movements in plants.

STAR★METHODS

Detailed methods are provided in the online version of this paper and include the following:

- KEY RESOURCES TABLE
- RESOURCE AVAILABILITY
  - Lead contact
  - Materials availability
  - Data and code availability
- EXPERIMENTAL MODEL AND SUBJECT DETAILS
  - Plant materials and growth conditions
- METHOD DETAILS
  - Ancestral character-state reconstruction
  - Microscopy, SEM, and histology
  - Cell measurement
  - Computational modeling
  - DGE profiling
  - Phylogenetic analysis and gene isolation
  - Expression and functional studies
  - Auxin application
- QUANTIFICATION AND STATISTICAL ANALYSIS

SUPPLEMENTAL INFORMATION

Supplemental information can be found online at https://doi.org/10.1016/j.cub.2024.01.004.

ACKNOWLEDGMENTS

We would like to thank Wengen Zhang, Baoqing Ding, Hongyan Shan, Xuehao Fu, Elena M. Kramer, Shuixian Li, and Jiannan Fan for valuable comments and suggestions; Cèsar Blanché, Joan Simon, and Maria Bosch for providing the morphological information of subg. *Delphinium*; Li Yuan and the Horticulture Science Research Center of Northwest A&F University for technical assistance on semi-thin sectioning; and the editors and the three anonymous reviewers for their insightful suggestions. This work was supported by a National Natural Science Foundation of China (31970247), the Qin Chuangyuan High-level Innovation and Entrepreneurship Talent Program (2021QCYRC4-51), and the Fundamental Research Funds for Northwest A&F University. This paper is in memory of botanist Dr. Yi Ren (1959–2019).

AUTHOR CONTRIBUTIONS

R.Z., L.G., and H.Z. designed the research. H.Z., F.X., and Y.W. provided the microscopy results. F.X., F.J., and P.-E.D. collected the morphological character in terms of the presence or absence of petal asymmetric bending. F.X., L.G., and R.Z. carried out the evolutionary and phylogenetic analyses. J.C. and H.Z. conducted the computational modeling. H.Z., P.Z., and Y.X. performed *in situ* hybridization, RT-qPCR, VIGS, and IAA treatment experiments. R.Z., L.G., and H.Z. analyzed the RNA-seq data. R.Z., L.G., H.Z., X.D., and H.K. contributed to the writing and revision of the manuscript. All authors read and approved the final paper.

DECLARATION OF INTERESTS

The authors declare no competing interests.

Received: November 9, 2023
Revised: December 13, 2023
Accepted: January 2, 2024
Published: January 24, 2024

REFERENCES

1. Darwin, C. (1880). The Power of Movement in Plants (Cambridge University Press).
2. Sisodia, R., and Bhatla, S.C. (2018). Plant movements. In Plant Physiology, Development and Metabolism, S.C. Bhatla, and M.A. Lal, eds. (Springer, Singapore), pp. 907–935.
3. Koller, D. (2011). The Restless Plant (Harvard University Press).
4. van Doorn, W.G., and Kamdee, C. (2014). Flower opening and closure: an update. J. Exp. Bot. *65*, 5749–5757.
5. van Doorn, W.G., and Van Meeteren, U. (2003). Flower opening and closure: a review. J. Exp. Bot. *54*, 1801–1812.
6. Liang, H., and Mahadevan, L. (2011). Growth, geometry, and mechanics of a blooming lily. Proc. Natl. Acad. Sci. USA *108*, 5516–5521.
7. Kaihara, S., and Takimoto, A. (1981). Physical basis of flower-opening in *Pharbitisl nil*. Plant Cell Physiol. *22*, 307–310.
8. Cheng, C., Yu, Q., Wang, Y., Wang, H., Dong, Y., Ji, Y., Zhou, X., Li, Y., Jiang, C.Z., Gan, S.S., et al. (2021). Ethylene-regulated asymmetric growth of the petal base promotes flower opening in rose (*Rosa hybrida*). Plant Cell *33*, 1229–1251.
9. Endress, P.K. (1999). Symmetry in flowers: diversity and evolution. Int. J. Plant Sci. *160*, S3–S23.
10. Jabbour, F., Ronse De Craene, L.P., Nadot, S., and Damerval, C. (2009). Establishment of zygomorphy on an ontogenic spiral and evolution of perianth in the tribe Delphinieae (Ranunculaceae). Ann. Bot. *104*, 809–822.
11. Jabbour, F., and Renner, S.S. (2012). Spurs in a spur: perianth evolution in the Delphinieae (Ranunculaceae). Int. J. Plant Sci. *173*, 1036–1054.
12. Zalko, J., Frachon, S., Morel, A., Deroin, T., Espinosa, F., Xiang, K.L., Wang, W., Zhang, W.G., Lang, S., Dixon, L., et al. (2021). Floral Organogenesis and Morphogenesis of *Staphisagria* (Ranunculaceae): Implications for the Evolution of Synorganized Floral Structures in Delphinieae. Int. J. Plant Sci. *182*, 59–70.
13. Zhang, W.G., Liu, Y.G., Nie, T.J., Guo, C.C., Qiu, L.H., Yang, G.Y., Jabbour, F., and Wang, W. (2021). Floral ontogeny of *Delphinium anthriscifolium* (Ranunculaceae) and development of intrafloral and symmetrical resupinated organs. Bot. J. Linn. Soc. *198*, 1–13.
14. Hou, Q.Z., Shao, W.J., Ehmet, N., Yang, G., Zhong, Y.Q., Min, W.R., Xu, Y.F., and Gao, R.C. (2022). The biomechanical screening game between visitor power and staminode operative strength of *Delphinium caeruleum* (Ranunculaceae). Plants (Basel) *11*, 2319.
15. Müller, H. (1883). The Fertilisation of Flowers (MacMillan & Co.).
16. Blanché, C. (1990). *Delphinium* L. subgen. *Delphinium*: origin and evolutionary trends. Collect. Bot. *19*, 75–96.
17. Jabbour, F., and Renner, S.S. (2012). A phylogeny of Delphinieae (Ranunculaceae) shows that *Aconitum* is nested within *Delphinium* and that Late Miocene transitions to long life cycles in the Himalayas and Southwest China coincide with bursts in diversification. Mol. Phylogenet. Evol. *62*, 928–942.
18. Xiang, K.L., Aytaç, Z., Liu, Y., Espinosa, F., Jabbour, F., Byng, J.W., Zhang, C.F., Erst, A.S., and Wang, W. (2017). Recircumscription of *Delphinium* subg. *Delphinium* (Ranunculaceae) and implications for its biogeography. Taxon *66*, 554–566.
19. Zhai, W., Duan, X.S., Zhang, R., Guo, C.C., Li, L., Xu, G.X., Shan, H.Y., Kong, H.Z., and Ren, Y. (2019). Chloroplast genomic data provide new and robust insights into the phylogeny and evolution of the Ranunculaceae. Mol. Phylogenet. Evol. *135*, 12–21.
20. DuPasquier, P.E., Andro-Durand, V., Batory, L., Wang, W., and Jabbour, F. (2021). Nomenclatural revision of *Delphinium* subg. *Consolida* (DC.) Huth (Ranunculaceae). PhytoKeys *180*, 81–110.
21. Zhao, H.Q., Liao, H., Li, S.X., Zhang, R., Dai, J., Ma, P., Wang, T., Wang, M.M., Yuan, Y., Fu, X.H., et al. (2023). Delphinieae flowers originated from the rewiring of interactions between duplicated and diversified floral organ identity and symmetry genes. Plant Cell *35*, 994–1012.
22. Kennaway, R., Coen, E., Green, A., and Bangham, A. (2011). Generation of diverse biological forms through combinatorial interactions between tissue polarity and growth. PLoS Comput. Biol. *7*, e1002071.
23. Rebocho, A.B., Southam, P., Kennaway, J.R., Bangham, J.A., and Coen, E. (2017). Generation of shape complexity through tissue conflict resolution. eLife *6*, e20156.
24. Cheng, J., Yao, X., Li, X., Yue, L., Duan, X., Li, B., Fu, X., Li, S., Shan, H., Yin, X., et al. (2023). Diversification of ranunculaceous petals in shape supports a generalized model for plant lateral organ morphogenesis and evolution. Sci. Adv. *9*, eadf8049.
25. Corley, S.B., Carpenter, R., Copsey, L., and Coen, E. (2005). Floral asymmetry involves an interplay between TCP and MYB transcription factors in *Antirrhinum*. Proc. Natl. Acad. Sci. USA *102*, 5068–5073.
26. Nakata, M., Matsumoto, N., Tsugeki, R., Rikirsch, E., Laux, T., and Okada, K. (2012). Roles of the middle domain-specific *WUSCHEL-RELATED HOMEOBOX* genes in early development of leaves in *Arabidopsis*. Plant Cell *24*, 519–535.
27. Andres, R.J., Coneva, V., Frank, M.H., Tuttle, J.R., Samayoa, L.F., Han, S.W., Kaur, B., Zhu, L., Fang, H., Bowman, D.T., et al. (2017). Modifications to a *LATE MERISTEM IDENTITY1* gene are responsible for the major leaf shapes of Upland cotton (*Gossypium hirsutum* L.). Proc. Natl. Acad. Sci. USA *114*, E57–E66.
28. Hofer, J., Turner, L., Moreau, C., Ambrose, M., Isaac, P., Butcher, S., Weller, J., Dupin, A., Dalmais, M., Le Signor, C., et al. (2009). *Tendrilless* regulates tendril formation in pea leaves. Plant Cell *21*, 420–428.
29. Vlad, D., Kierzkowski, D., Rast, M.I., Vuolo, F., Dello Ioio, R., Galinha, C., Gan, X., Hajheidari, M., Hay, A., Smith, R.S., et al. (2014). Leaf shape evolution through duplication, regulatory diversification, and loss of a homeobox gene. Science *343*, 780–783.
30. Zhang, R., Fu, X.H., Zhao, C.Y., Cheng, J., Liao, H., Wang, P.P., Yao, X., Duan, X.S., Yuan, Y., Xu, G.X., et al. (2020). Identification of the key regulatory genes involved in elaborate petal development and specialized character formation in *Nigella damascena* (Ranunculaceae). Plant Cell *32*, 3095–3112.
31. Zhao, J.L., Pan, J.S., Guan, Y., Zhang, W.W., Bie, B.B., Wang, Y.L., He, H.L., Lian, H.L., and Cai, R. (2015). *Micro-trichome* as a class I homeodomain-leucine zipper gene regulates multicellular trichome development in *Cucumis sativus*. J. Integr. Plant Biol. *57*, 925–935.
32. Mara, C.D., and Irish, V.F. (2008). Two GATA transcription factors are downstream effectors of floral homeotic gene action in Arabidopsis. Plant Physiol. *147*, 707–718.
33. Jonsson, K., Ma, Y., Routier-Kierzkowska, A.L., and Bhalerao, R.P. (2023). Multiple mechanisms behind plant bending. Nat. Plants *9*, 13–21.

34. Wang, W.T. (2019). A revision of the genus *Delphinium* (Ranunculaceae) of China (I). Guihaia *39*, 1425–1446.

35. Hodges, S.A. (1997). Floral nectar spurs and diversification. Int. J. Plant Sci. *158*, S81–S88.

36. Hodges, S.A., and Arnold, M.L. (1995). Spurring plant diversification: are floral nectar spurs a key innovation? Proc. R. Soc. Lond. B *262*, 343–348.

37. Crawford, B.C., Nath, U., Carpenter, R., and Coen, E.S. (2004). CINCINNATA controls both cell differentiation and growth in petal lobes and leaves of Antirrhinum. Plant Physiol. *135*, 244–253.

38. Rebocho, A.B., Kennaway, J.R., Bangham, J.A., and Coen, E. (2017). Formation and shaping of the *Antirrhinum* flower through modulation of the *CUP* boundary gene. Curr. Biol. *27*, 2610–2622.e3.

39. Berry, E., Choudhary, A.K., and Geeta, R. (2022). Why do some funneliform flowers have petal folds accompanied with hierarchical surface microstructure? Evol. Ecol. *37*, 385–399.

40. Vuolo, F., Kierzkowski, D., Runions, A., Hajheidari, M., Mentink, R.A., Gupta, M.D., Zhang, Z., Vlad, D., Wang, Y., Pecinka, A., et al. (2018). LMI1 homeodomain protein regulates organ proportions by spatial modulation of endoreduplication. Genes Dev. *32*, 1361–1366.

41. Jonsson, K., Lathe, R.S., Kierzkowski, D., Routier-Kierzkowska, A.L., Hamant, O., and Bhalerao, R.P. (2021). Mechanochemical feedback mediates tissue bending required for seedling emergence. Curr. Biol. *31*, 1154–1164.e3.

42. Žádníková, P., Petrásek, J., Marhavy, P., Raz, V., Vandenbussche, F., Ding, Z., Schwarzerová, K., Morita, M.T., Tasaka, M., Hejátko, J., et al. (2010). Role of PIN-mediated auxin efflux in apical hook development of *Arabidopsis thaliana*. Development *137*, 607–617.

43. Cheng, Y., Dai, X., and Zhao, Y. (2006). Auxin biosynthesis by the YUCCA flavin monooxygenases controls the formation of floral organs and vascular tissues in *Arabidopsis*. Genes Dev. *20*, 1790–1799.

44. Gälweiler, L., Guan, C., Müller, A., Wisman, E., Mendgen, K., Yephremov, A., and Palme, K. (1998). Regulation of polar auxin transport by AtPIN1 in *Arabidopsis* vascular tissue. Science *282*, 2226–2230.

45. Li, H., Johnson, P., Stepanova, A., Alonso, J.M., and Ecker, J.R. (2004). Convergence of signaling pathways in the control of differential cell growth in *Arabidopsis*. Dev. Cell *7*, 193–204.

46. Okada, K., Ueda, J., Komaki, M.K., Bell, C.J., and Shimura, Y. (1991). Requirement of the auxin polar transport system in early stages of *Arabidopsis* floral bud formation. Plant Cell *3*, 677–684.

47. Rawat, R., Schwartz, J., Jones, M.A., Sairanen, I., Cheng, Y., Andersson, C.R., Zhao, Y., Ljung, K., and Harmer, S.L. (2009). REVEILLE1, a Myb-like transcription factor, integrates the circadian clock and auxin pathways. Proc. Natl. Acad. Sci. USA *106*, 16883–16888.

48. Mazzella, M.A., Casal, J.J., Muschietti, J.P., and Fox, A.R. (2014). Hormonal networks involved in apical hook development in darkness and their response to light. Front. Plant Sci. *5*, 52.

49. Kolattukudy, P.E. (1980). Biopolyester membranes of plants: cutin and suberin. Science *208*, 990–1000.

50. Yeats, T.H., and Rose, J.K. (2013). The formation and function of plant cuticles. Plant Physiol. *163*, 5–20.

51. Smyth, D.R. (2016). Helical growth in plant organs: mechanisms and significance. Development *143*, 3272–3282.

52. Thitamadee, S., Tuchihara, K., and Hashimoto, T. (2002). Microtubule basis for left-handed helical growth in *Arabidopsis*. Nature *417*, 193–196.

53. Furutani, I., Watanabe, Y., Prieto, R., Masukawa, M., Suzuki, K., Naoi, K., Thitamadee, S., Shikanai, T., and Hashimoto, T. (2000). The *SPIRAL* genes are required for directional control of cell elongation in *Arabidopsis thaliana*. Development *127*, 4443–4453.

54. Saffer, A.M., Carpita, N.C., and Irish, V.F. (2017). Rhamnose-containing cell wall polymers suppress helical plant growth independently of microtubule orientation. Curr. Biol. *27*, 2248–2259.e4.

55. Gerbode, S.J., Puzey, J.R., McCormick, A.G., and Mahadevan, L. (2012). How the cucumber tendril coils and overwinds. Science *337*, 1087–1091.

56. Hofhuis, H., Moulton, D., Lessinnes, T., Routier-Kierzkowska, A.L., Bomphrey, R.J., Mosca, G., Reinhardt, H., Sarchet, P., Gan, X., Tsiantis, M., et al. (2016). Morphomechanical innovation drives explosive seed dispersal. Cell *166*, 222–233.

57. Wickham, H. (2016). ggplot2: Elegant Graphics for Data Analysis, Second Edition (Springer).

58. Nguyen, L.T., Schmidt, H.A., von Haeseler, A., and Minh, B.Q. (2015). IQ-TREE: a fast and effective stochastic algorithm for estimating maximum-likelihood phylogenies. Mol. Biol. Evol. *32*, 268–274.

59. Maddison, W.P., and Maddison, D.R. (2023). Mesquite: a modular system for evolutionary analysis. Version 3.81. http://www.mesquiteproject.org.

60. Grabherr, M.G., Haas, B.J., Yassour, M., Levin, J.Z., Thompson, D.A., Amit, I., Adiconis, X., Fan, L., Raychowdhury, R., Zeng, Q., et al. (2011). Full-length transcriptome assembly from RNA-Seq data without a reference genome. Nat. Biotechnol. *29*, 644–652.

61. Fu, L.M., Niu, B.F., Zhu, Z.W., Wu, S.T., and Li, W.Z. (2012). CD-HIT: accelerated for clustering the next-generation sequencing data. Bioinformatics *28*, 3150–3152.

62. Quesneville, H., Bergman, C.M., Andrieu, O., Autard, D., Nouaud, D., Ashburner, M., and Anxolabehere, D. (2005). Combined evidence annotation of transposable elements in genome sequences. PLoS Comput. Biol. *1*, 166–175.

63. Kim, D., Pertea, G., Trapnell, C., Pimentel, H., Kelley, R., and Salzberg, S.L. (2013). TopHat2: accurate alignment of transcriptomes in the presence of insertions, deletions and gene fusions. Genome Biol. *14*, R36.

64. Li, B., and Dewey, C.N. (2011). RSEM: accurate transcript quantification from RNA-Seq data with or without a reference genome. BMC Bioinformatics *12*, 323.

65. Love, M.I., Huber, W., and Anders, S. (2014). Moderated estimation of fold change and dispersion for RNA-seq data with DESeq2. Genome Biol. *15*, 550.

66. Yu, X., Duan, X., Zhang, R., Fu, X., Ye, L., Kong, H., Xu, G., and Shan, H. (2016). Prevalent exon-intron structural changes in the *APETALA1/FRUITFULL*, *SEPALLATA*, *AGAMOUS-LIKE6*, and *FLOWERING LOCUS C* MADS-box gene subfamilies provide new insights into their evolution. Front. Plant Sci. *7*, 598.

67. Wang, P., Liao, H., Zhang, W., Yu, X., Zhang, R., Shan, H., Duan, X., Yao, X., and Kong, H. (2015). Flexibility in the structure of spiral flowers and its underlying mechanisms. Nat. Plants *2*, 15188.

68. Livak, K.J., and Schmittgen, T.D. (2001). Analysis of relative gene expression data using real-time quantitative PCR and the $2^{-\Delta\Delta CT}$ method. Methods *25*, 402–408.

STAR★METHODS

KEY RESOURCES TABLE

REAGENT or RESOURCE	SOURCE	IDENTIFIER
Antibodies		
Anti-DIG	Roche	CAT# 11093274910; RRID: AB_514497
Bacterial and virus strains		
Escherichia coli DH5α	WEIDI	CAT# DL1001
Agrobacterium tumefaciens GV3101	WEIDI	CAT# AC1001
Biological samples		
Delphinium anthriscifolium	Taibai MT, Shaanxi, China	N/A
Chemicals, peptides, and recombinant proteins		
Indole-3-acetic acid (IAA)	Solarbio	CAT# I8020
Toluidine Blue	Servicebio	CAT# GP1032
Technovit 7100 resin	Kulzer GmbH	CAT# No.37100
Lanolin anhydrous	Macklin	CAT# 8006-54-0
T7 RNA Polymerase	Roche	CAT# 10881767001
Critical commercial assays		
RNAprep Pure Plant Kit	TIANGEN	CAT# 4992239
pEASY®-Blunt Cloning Kit	TransGen	CAT# CB101-01
ChamQ SYBR qPCR Master Mix	Vazyme	CAT# Q311-02
Deposited data		
RNA-seq data	This paper	PRJNA1051014
CDS sequence of *DeanLMI1*	This paper	OR902771
Oligonucleotides		
Primer for in situ hybridization: *DeanLMI1*-F (5'-ACGACACGCTGAAGAAGGAG-3')	This paper	N/A
Primer for in situ hybridization: *DeanLMI1*-R (5'-TGTTGGGATGCCCCGACGC-3')	This paper	N/A
Primer for qRT: *Actin*-qRT-F (5'-CCGTTCTGCTGTGGTTGTG-3')	This paper	N/A
Primer for qRT: *Actin*-qRT-R (5'-GTGTTGGACTCTGGTGATGG-3	This paper	N/A
Primer for qRT: *DeanLMI1*-qRT-F (5'-ATGGCTTGGAGTGCGAACC-3')	This paper	N/A
Primer for qRT: *DeanLMI1*-qRT-R (5'-CTCGGGATTCTCATGCTCGC-3')	This paper	N/A
Primer for VIGS: *DeanANS*-VIGS-F (5'-GGTCTAGATTTGGGATTGGAAGACGGCA-3')	This paper	N/A
Primer for VIGS: *DeanANS*-VIGS-R (5'-AAGGATCCACCCATTTGCCTTCGGTGAA-3')	This paper	N/A
Primer for VIGS: *DeanLMI1*-VIGS-F (5'-GGGGATCCAGGGCATCAACAAAGCA-3').	This paper	N/A
Primer for VIGS: *DeanLMI*-VIGS-R (5'-GGGGTACCAGTGTAGCCATCCATAAGC-3').	This paper	N/A
Recombinant DNA		
TRV2-*DeanANS*	This paper	N/A
TRV2-*DeanANS*-*DeanLMI1*	This paper	N/A
Software and algorithms		
ImageJ	National Institutes of Health	https://imagej.nih.gov/ij/

(*Continued on next page*)

Continued

REAGENT or RESOURCE	SOURCE	IDENTIFIER
GraphPad Prism 6	GraphPad	https://www.graphpad.com/resources
R	R Core Team	http://www.r-project.org
R package: ggplot2 (version 3.3.5)	Wickham[57]	https://ggplot2.tidyverse.org/
GFtbox	BanghamLab	https://github.com/JIC-Enrico-Coen/GrowthToolbox
MATLAB	Mathworks	https://www.mathworks.com/products/matlab.html
MESQUITE v.3.81	Mesquite	http://www.mesquiteproject.org
IQ-TREE1.6.10	Nguyen et al.[58]	https://github.com/Cibiv/IQ-TREE/releases/tag/v1.6.10

RESOURCE AVAILABILITY

Lead contact

Further information and requests for resources and reagents should be directed to and will be fulfilled by the lead contact, Rui Zhang (ruizhang@nwafu.edu.cn).

Materials availability

All unique/stable reagents generated in this study are available from the lead contact.

Data and code availability

- Clean reads of the RNA-seq data in this work are deposited at BioProject in NCBI under the accession number (PRJNA1051014) (https://www.ncbi.nlm.nih.gov/bioproject/?term=PRJNA1051014).
- The accession number for the *DeanLMI1* sequence of *D. anthriscifolium* reported in this work is GenBank: OR902771 (https://www.ncbi.nlm.nih.gov/nuccore/OR902771).
- Any additional information required to reanalyze the data reported in this paper is available from the lead contact upon request.

EXPERIMENTAL MODEL AND SUBJECT DETAILS

Plant materials and growth conditions

Seeds of *D. anthriscifolium* were collected from Taibai Mountain, Shaanxi (China), sown in soil (vermiculite: nutrient soil = 1:1) and cultivated under controlled conditions with a 14 h light (20000 Lux) and 10 h dark photoperiod at 24°C and 60% relative humidity.

METHOD DETAILS

Ancestral character-state reconstruction

To infer the ancestral character state of presence/absence of petal asymmetric bending shown in Figures 1A and S2, we employed MESQUITE v.3.81 with a likelihood model.[59] The matrix of morphological characters for ancestral character state reconstruction analyzed in this study is presented in Table S1.

Microscopy, SEM, and histology

Typical mature flowers per species were photographed using an EOS 760D digital camera (Canon, Tokyo, Japan) paired with a Canon EF-S 60mm f/2.8 lens. Petals were dissected with an Olympus SZX16 stereomicroscope (Olympus, Tokyo, Japan) and imaged with an OLYMPUS SC180 digital camera.

For SEM analysis shown in Figures 2, 3, and 7, as well as Figures S3, S4, S6, and S7, samples were prepared following the previously described method,[21] with slight modifications. Specifically, petals at different developmental stages were dissected under a stereomicroscope, fixed in FAA solution (3.7% formaldehyde, 5% acetic acid, and 50% ethanol), dehydrated using a graded series of water-ethanol, and dried with a CO_2 critical-point dryer. The prepared samples were then mounted on aluminum stubs, subjected to gold sputter coating, and observed under a S-3400N scanning electron microscope (HITACHI, Tokyo, Japan).

For histological observations shown in Figures 2G, 3 (right column), 7M, 7N, and S4 (left column), semi-thin sections of petals were prepared according to the protocol described in the instruction manual of Technovit 7100 resin (Kulzer GmbH, Hanau, Germany). Serial sections of 5 μm in thickness were prepared using a Leica RM2265 Automated microtome (Leica, Wetzlar, Germany). After

rehydration, sections were stained with 0.5% toluidine blue (Servicebio, Wuhan, China) and then photographed using an OLYMPUS BX51 optical microscope (Olympus, Tokyo, Japan) and an OLYMPUS DP72 digital camera.

Cell measurement

Cell counts and size measurements shown in Figures 2, 3, and 7, as well as Figures S3, S4, S6, and S7, were determined using ImageJ and Photoshop software. The cell size data in SEM assays and cell number data in semi-thin section assays were plotted using GraphPad Prism. The cell width data in semi-thin section assays were graphed using the geom_smooth function from the ggplot2 package in R software.

Computational modeling

For the computational modeling shown in Figure 4, all models were performed with *GFtbox* (https://github.com/JIC-Enrico-Coen/GrowthToolbox), which is an implemented toolbox in MATLAB (https://www.mathworks.com/products/matlab.html). The petal models were built based on a previous reported modeling system.[24] Code is available in the supplementary files and at the GitHub repository (https://github.com/Darwincj/GFtbox_petal_folding). Growth rate regulatory networks for each model at later stage are listed below. *kapar* and *kbpar* represent *K*pd on abaxial and adaxial side, respectively. *kaper* and *kbper* represent *K*per on abaxial and adaxial side, respectively.

Specified growth rates per time unit for the default model in (Figures 4C–4E) were:

kapar = 0.12 * pro(0.2, i_{mid}) * inh(0.5, s_{asym}) * inh(5, i_{sinus})

kaper = 0.08 * inh(10, i_{stk}) * pro(0.8, s_{asym}) * inh(5, i_{sinus})

kbpar = 0.12 * pro(0.2, i_{mid}) * inh(0.5, s_{asym}) * inh(5, i_{sinus})

kbper = 0.08 * inh(10, i_{stk}) * pro(0.8, s_{asym}) * inh(5, i_{sinus})

Specified growth rates per time unit for the model in (Figures 4F–4H) were:

kapar = 0.12 * pro(0.2, i_{mid}) * inh(0.5, s_{asym}) * inh(5, i_{sinus})

kaper = 0.08 * inh(10, i_{stk}) * pro(0.8, s_{asym}) * inh(5, i_{sinus}) * pro(0.3, s_{fold})

kbpar = 0.12 * pro(0.2, i_{mid}) * inh(0.5, s_{asym}) * inh(5, i_{sinus})

kbper = 0.08 * inh(10, i_{stk}) * pro(0.8, s_{asym}) * inh(5, i_{sinus}) * pro(0.3, s_{fold})

Specified growth rates per time unit for the model in (Figures 4I–4K) were:

kapar = 0.12 * pro(0.2, i_{mid}) * inh(0.5, s_{asym}) * inh(5, i_{sinus})

kaper = 0.08 * inh(10, i_{stk}) * pro(0.8, s_{asym}) * inh(5, i_{sinus})

kbpar = 0.12 * pro(0.2, i_{mid}) * inh(0.5, s_{asym}) * inh(5, i_{sinus})

kbper = 0.08 * inh(10, i_{stk}) * pro(0.8, s_{asym}) * inh(5, i_{sinus}) * pro(0.3, s_{fold})

DGE profiling

To generate a reference transcriptome of *D. anthriscifolium*, total RNAs of floral buds, bracts and leaves at different developmental stages were separately extracted using the RNAprep Pure Plant Plus Kit (TIANGEN, Beijing, China) and then pooled for library construction. Paired-end 150-bp reads were sequenced on the Illumina NovaSeq6000 platform (Novogene, Beijing, China), and the clean reads were assembled into transcripts using Trinity.[60] Protein-coding unigenes were predicted by ANGEL (https://github.com/PacificBiosciences/ANGEL) and filtered by CD-HIT and all-by-all BLASTN.[61,62]

Next, for the DGE profiling of floral organs, leaves and bracts at different developmental stages shown in Figures 7A–7C, 30 samples, each with three or four biological replicates except for those at S9 that contained two replicates due to the limited number of floral buds, were collected. For the DGE profiling of VIGS-treated plants shown in Figure 5A, the mock and *ans-lmi1* strongly silenced petals at S12 of floral development, each with two replicates, were collected. A total of 89 DGE profiles were separately subjected to RNA extraction, library construction and sequencing as described above. Clean reads of each sample was mapped to the reference transcriptome by TopHat2 and fragments per kilobase per million mapped reads (FPKM) values were calculated using RSEM.[63,64] The average FPKM value of the replicates was used as the gene expression level in the corresponding sample. The quality of the DGE profiles was evaluated based on reads mapping rates and the PCC (Pearson correlation coefficients) among the biological replicates.

The overall comparisons of the expression profiles between samples were conducted using PCC, SCC (Spearman Correlation Coefficient), and PCA (Principal Component Analysis) analyses (Figures S5A and S5B). PCC and SCC were conducted in R using the cor.test function with Pearson and Spearman methods, respectively. PCA was performed using the prcomp function in R with original FPKM values as inputs.

Expressed genes (FPKM $\geq$ 1.0 in at least one sample), specifically expressed genes (FPKM $\geq$ 1.0 exclusively in a specific organ) shown in Figure S5C and preferentially expressed genes (FPKM in one organ $\geq$ 2 times FPKM in any other organ) shown in Figure 5B were defined following the method described by Zhang et al.[30] Differentially expressed gene analyses between spurred dorsal and lateral nonspurred petals shown in Figures 5C and S5D were conducted using DESeq2 based on the petal specifically and preferentially expressed genes, applying a fold change cut-off of 2 and a *P*-value threshold of 0.05 with Benjamini-Hochberg adjustment.[65] Differentially expressed gene analysis between the mock and *ans-lmi1* petals shown in Figures 5C and S7A was performed using the LIMMA package in R software, with a screening threshold as described above.

Phylogenetic analysis and gene isolation

For the phylogenetic analysis shown in Figure S6A, coding sequences of putative *LMI1*-like genes from representative species were retrieved through BLAST searches against publicly available databases. Sequence alignment and adjustment were conducted as previously described by Yu et al.[66] The alignable nucleotide matrix (Data S3A) was used for phylogenetic reconstruction in IQ-TREE1.6.10 using the maximum-likelihood method with the best-fit model of TIM2+F+I+G4 and the 1000 bootstrap replicates.[58] The tree topology in a Newick format can be found in Data S3B.

Expression and functional studies

The CDS sequence of *DeanLMI1* was amplified, inserted into the *pEASY*®-Blunt E1 cloning vector (TransGen, Beijing, China), and verified by sequencing. The expression patterns of *DeanLMI1* as revealed by mRNA *in situ* hybridization (Figure 6) followed the procedures described by Wang et al.[67] The antisense probe of *DeanLMI1* was obtained through RNA transcription using the *DeanLMI1*-R primer containing the T7 promoter in combination with the *DeanLMI1*-F primer (see key resources table).

The RT-qPCR experiments shown in Figures 5F and S6K were conducted using the ChamQ SYBR qPCR Master Mix (Vazyme, Nanjing, China) on a QuantStudio3 instrument (Life Technologies, California, USA). The RT-qPCR primers, including Actin-qRT-F/R and *DeanLMI1*-qRT-F/R (see key resources table), were employed alongside *in situ* hybridization to assess *DeanLMI1* expression. Gene expression was determined using the $2^{-\triangle\triangle CT}$ relative quantification method.[68]

For the functional studies of *DeanLMI1* shown in Figures 7, S6E, and S6F, we applied VIGS experiment. The detailed procedure of construct transformation and plant treatment followed the previous study.[67] The VIGS vectors of *DeanANS* and *DeanLMI1* were obtained by primers for *DeanANS*-VIGS-F/R and *DeanLMI1*-VIGS-F/R (see key resources table). A total of eight rounds of treatments were conducted with TRV2-*DeanANS*-*DeanLMI1* construct, with the TRV2-*DeanANS* construct being used as the mock (Table S2). Flowers showing phenotypic changes were photodocumented. The morphology, micromorphology, and histology of flowers with visible phenotypic changes were investigated as described above. Silencing efficiency was assessed by RT-qPCR as described by Wang et al.,[67] using cDNAs from petals of WT, mock and *ans-lmi1* petals at S12 as templates.

Auxin application

For the IAA application experiment shown in Figure S7, indole-3-acetic acid (IAA; Solarbio, Beijing, China) was dissolved in liquid lanolin (Macklin, Shanghai, China) at 40°C to achieve a final concentration of 100 mM and was cooled to room temperature. The paste was applied to the abaxial surface of the lateral petals using a fine paintbrush, with pure lanolin as a control. A total of 85 flowers from 10 plants and 40 flowers from 5 plants were treated with 100 mM paste and pure lanolin, respectively. All flowers were treated twice, once at developmental S11 and again at S14, ensuring uniform size at each treatment.

QUANTIFICATION AND STATISTICAL ANALYSIS

The paired two-sample analysis of means T-test was used to assess the significant differences between samples in SEM and semi-thin section assays. Statistical significance is denoted as follows: "ns" ($p > 0.05$), "*" ($p < 0.05$), "**" ($p < 0.01$), and "***" ($p < 0.001$).